

Numerical assessment of FRP retrofitting systems for reinforced concrete elements

V.C. Rougier^a, B.M. Luccioni^{a,b,*}

^a Structures Institute, National University of Tucumán, Av. Pres. Gral. J. A. Roca 1800, San Miguel de Tucumán, T4000ACR Tucumán, Argentina

^b CONICET, Av. Rivadavia 1917, Ciudad de Buenos Aires, C1033AAJ, Buenos Aires, Argentina

Received 9 May 2005; received in revised form 11 August 2006; accepted 1 September 2006

Available online 27 October 2006

Abstract

During their service life reinforced concrete structures can be exposed to mechanical loads and aggressive chemical or thermal agents that produce degradation of their mechanical properties. This results in a loss of security and usually requires a prompt repair or retrofitting in order to preserve the structural serviceability. In this case, the aid of a numerical tool for the assessment of different retrofit and repair systems would be valuable. Nowadays, analytical and numerical capacity for the assessment of this type of systems is still limited.

A numerical model that can be used for the assessment of retrofit and repair systems based on the use of FRP for reinforced concrete columns and beams is presented in this paper. A plastic damaged model that reproduces the behaviour even under high confinement pressures is used for concrete.

Application examples concerning the behaviour of reinforced concrete columns and beams retrofitted with FRP are included in the paper. The comparison with experimental results shows the ability of the proposed model to reproduce the problem simulated.

© 2006 Elsevier Ltd. All rights reserved.

Keywords: Reinforced concrete; Fiber reinforced plastic; Retrofitting; Confinement; Flexural reinforcement; Numerical model; Plasticity; Damage; Composites

1. Introduction

Strengthening reinforced concrete (RC) structures with Fibre-Reinforced Polymer (FRP) composites is becoming an attractive alternative for the construction industry and rehabilitation of existing reinforced concrete (RC) structures [1]. Rehabilitation of these structures can be in the form of strengthening of structural members, repair of damaged structures, or retrofitting for seismic deficiencies. In any case, composite materials are an excellent option to be used as external reinforcement because of their high tensile strength, light weight, resistance to corrosion, high durability and easy installation [2].

Externally bonded FRP reinforcement has been shown to be applicable for the strengthening of many types of RC structures such as columns, beams, slabs, walls, tunnels, chimneys and silos. It can be used to improve flexural and shear capacities

and also to provide confinement and ductility to compression members [2].

It has been shown that wrapping FRP composite sheets around the perimeter of both circular and rectangular concrete columns improves ductility and strength [3]. The actual analytical ability to quantify the behaviour of FRP confined concrete columns is rather limited, especially with respect to ductility. As a result, code requirements on reinforcement may be too conservative in most cases, and may still be insufficient for some situations of extensive deformations caused by severe earthquake loads [4].

In the case of reinforced concrete beams, reinforcement with composite materials enhances the flexural capacity and shear strength. Nevertheless, in order to better understand the flexural behaviour of these beams, a complementary analysis is necessary. The reinforcement is made of several layers (steel bars, adhesive, FRP). The behaviour of steel in concrete is well known, but the association of concrete with FRP is difficult to analyze as it implies an adhesive layer [5].

Although experimental data is valuable in understanding the behaviour of this strengthening system, analytical and

* Corresponding address: Country Las Yungas, (4107) Yerba Buena, Tucumán, Argentina. Tel.: +54 381 4257511; fax: +54 381 4364087.

E-mail address: bluccioni@herrera.unt.edu.ar (B.M. Luccioni).

URL: <http://www.herrera.unt.edu.ar/iest/> (B.M. Luccioni).

numerical solutions are also needed to further understand and predict the behaviour and failure mechanism of the strengthened beams [1]. Experimental studies have shown that plated beams generally fail in a brittle and sudden manner and therefore they are not able to reach their ultimate flexural capacity [6]. Significant efforts have recently been made to investigate and predict these kinds of failures that include the ‘peeling off’ of the FRP plate and shear failure of the concrete layer between the plate and longitudinal reinforcement, but this is not an easy task [7]. Although many finite element analyses on plated RC beams have been carried out, little success has been achieved in simulating brittle failures [6]. This is mainly due to the complexity of the problem. Yang et al. [8] have developed a discrete crack model based on a finite element analysis method for RC beam reinforced with fibre reinforced polymer plates, which can simulate multiple discrete crack propagation during the whole loading process until the structures collapse. Perera et al. [9] have proposed a nonlinear numerical model based on damage mechanics, that permits consideration of the position and increase of concrete cracks which have a very important influence on the behaviour of strengthened beams. The model also affects the stress distribution and the failure mechanism. Lopez [1] has developed a numerical model approach that can reproduce the global load–deflection response of RC beams strengthened with CFRP laminates and the changes in strain along the length of the FRP laminates. Buyle-Bodin et al. [10] have proposed a finite element model to analyze and predict the flexural behaviour of strengthened and repaired beams.

On the other hand, theoretical models for prediction of the behaviour of laminate strengthened beams have been proposed [11–13]. These models usually assume strain compatibility, perfect bond between laminate and concrete, no tensile strength in concrete and the fact that the sections remain plain before and after bending. They also assume that the beam fails by either concrete compression or tensile failure of the laminate. Theoretical models can predict, with reasonable limits, the path of the load–deflection curve and strains (both laminate and concrete), but generally they are not able to reproduce the ultimate moments for strengthened beams.

The behaviour of reinforced concrete columns and beams externally reinforced with FRP is numerically modelled in this paper. First a brief description of the behaviour of reinforced concrete columns and beams retrofitted with FRP is presented. Then, the numerical model developed for the evaluation of concrete and the retrofitting system is described. The behaviour of reinforced concrete columns confined with FRP under uniaxial compression is numerically analyzed. Later the flexural behaviour of reinforced concrete beams strengthened with FRP is numerically studied. In all cases, numerically results are compared with the experimental ones in order to check the ability of the model presented to reproduce the system behaviour.

2. Retrofit of RC concrete elements with FRP

The structural effectiveness of FRPs in the rehabilitation of existing structural systems has repeatedly been demonstrated

with full or large-scale structural tests at the University of California, San Diego (UCSD) [14]. Carbon fabric overlays have been used to strengthen and retrofit reinforced and unreinforced masonry walls for seismic loads, as well as to restore and more than double the displacement capacity in the repair of a full-scale five-story reinforced masonry building tested to failure under simulated seismic loads. Carbon fibre overlays and strips have also been used to strengthen reinforced concrete slabs (with and without openings) and to strengthen large diameter prestressed concrete pipelines to restore loss of load (water pressure) carrying capacity due to corrosion of the prestressing wires. Bridge columns have been seismically retrofitted and repaired with fibreglass, carbon and hybrid composite jackets which were shown to be as effective as conventional steel jackets.

One of the methods for repair and retrofit of RC columns is fibre wrapping. The wrap enhances shear strength, axial strength and ductility of the column. It produces lateral strain restrictions that react to the Poisson-type lateral expansion tendencies of the concrete core, and generates side pressures, i.e. confinement. For flexural strengthening, fibre-reinforced polymer (FRP) sheets or near-surface-mounted FRP rods can be bonded to the column in the axial direction [15].

Unlike steel-encased concrete, response of FRP-encased concrete is almost bilinear with no descending branch [16]. This difference is due to the elastic behaviour of FRP composites. The response consists of three distinct regions. In the first region, the behaviour is similar to that of plain concrete, since lateral expansion of the core is insignificant. With the increase in microcracks, a transition zone is entered where the tube exerts a lateral pressure on the core to counteract the stiffness degradation of concrete. Finally, a third region is recognized in which the tube is fully activated and the stiffness is generally stabilized around a constant rate. The response in this region is mainly dependent on the stiffness of the tube.

Despite some volume expansion beyond the critical stress of confined concrete, the linearly increasing hoop stress of FRP eventually curtails the volume expansion and reverses its direction. It is clear that with an adequate amount of external fibre composites, lateral expansion of concrete can be effectively avoided. The dilatation rate remains constant during the early stages of loading, when concrete behaves elastically. As severe microcracks develop, the dilatation rate begins to increase. For unconfined concrete, with the growth of cracks opening dilatation becomes unstable. However, dilatation of FRP-encased concrete reaches a peak value after which it decreases and finally stabilizes at an asymptotic value.

The stress–strain path obtained for monotonically increasing load may serve as an envelope for the case of cyclic load characterized by loading and unloading branches forming loops. While the loops become wider beyond the peak strength of unconfined concrete, stiffness degradation is not as severe as that of steel-encased concrete [16,17].

Experimental tests performed on cylindrical specimens confined with CFRP and GFRP [15,18], have revealed that the failure modes are governed by the failure of the FRP and that the failure of CFRP is more sudden and explosive than that of

GFRP. For the same number of composite layers the CFRP [18] confinement gives a greater increase in strength and ductility.

Recent studies have also shown that external bonding of high-strength fibre-reinforced plastics (FRPs) to structural concrete flexural members is an effective method for increasing the structural capacity of such members. When effectively bonded to a flexural member, FRPs provide increased strength in the tension zone of a section that may have been determined to be deficient because of an inadequate design or a structural damage [19]. The increased in strength and ductility strongly depends on the unsheathed length and on the amount of CFRP laminates [5].

The study of this type of reinforcement has been centred on failure modes because the flexural strength of a section depends on the controlling failure mode [20]. From all these possible failure mechanisms, ACI 440 recommends concrete crushing as the most acceptable mode of failure.

In some particular cases, the strengthened beams showed a ductile behaviour, e.g. beams of higher shear-span to depth ratio ($a/d > 2.5$) and those provided with adequate end anchorage. The common dominant failure mode of RC beams strengthened with externally bonded CFRP laminates is the premature one, either laminates-end shear or concrete cover delamination. Therefore, the significant parameter affecting the failure behaviour of a strengthened beam is the shear stress in the adhesive layer between the external reinforcement and the concrete. The critical section is located at the longitudinal laminates-end region (cut-off point), where the shear stress concentration occurs. Such a shear stress is partially due to the variation of bending moment and the remaining part due to the introduction of forces in the anchoring zones [5]. Laminates-end shear starts at the cut-off point of the FRP and it is originated by a high concentration of normal (out of plane) and shear stresses. Concrete cover delamination starts from a flexural crack between the outermost crack and the maximum bending moment zone [7].

3. Modified plastic damage model for concrete

The model presented in this paper is thermodynamically consistent and comes from a generalization of plasticity theory [21–23] and isotropic damage theory. The plastic model has been adapted to be able to reproduce the behaviour of concrete under triaxial compression. Coupling of damage and plastic strains is achieved by solving both problems simultaneously [21,24]. In this way correct energy dissipation is also assured.

The use of a second degree function in the components of the stress tensor to define the elastic threshold and the ultimate strength allows the accurate reproduction of the variation of ultimate strength with hydrostatic pressure. The hardening variable has also been improved to reproduce energy dissipation in triaxial compression. The reproduction of dilatational response and ductility under high confinement pressure is achieved with the introduction of damage for levels of stress close to the ultimate strength in uniaxial compression.

The fulfillment of inequality of Clausius Planck for a given thermodynamic state is guaranteed if the stress is obtained as follows:

$$\sigma_{ij} = \frac{\partial \Psi^e}{\partial \varepsilon_{ij}^e} = (1-d) \frac{\partial \Psi^o}{\partial \varepsilon_{ij}^e} = C_{ijkl} \varepsilon_{kl}^e = (1-d) C_{ijkl}^o \varepsilon_{kl}^e \quad (1)$$

where σ_{ij} is the stress tensor, ε_{ij}^e is the elastic strains tensor, Ψ^e is the elastic part of free energy density, Ψ^o represents the elastic free energy density for the virgin material, $C_{ijkl}(d) = (1-d) C_{ijkl}^o$ is the secant constitutive tensor affected by the evolution of damage, C_{ijkl}^o is the elastic constitutive tensor of the virgin material. The damage variable d varies from 0, for the undamaged virgin material, to a maximum value d_c , for the completely damaged material, i.e. $0 \leq d \leq d_c$.

3.1. Plastic process

The plastic process is described by a generalization of classical plasticity theory that takes into account many aspects of geomaterials behaviour. Elastic threshold is defined by a yield function:

$$F^p(\sigma_{ij}; \kappa^p) = f^p(\sigma_{ij}) - K^p(\sigma_{ij}, \kappa^p) = 0 \quad (2)$$

where σ_{ij} is the stress tensor, $f(\sigma_{ij})$ is the equivalent stress, $K^p(\sigma_{ij}, \kappa^p)$ is the yielding threshold and κ^p is the plastic hardening variable.

The following rule is used for the evolution of plastic strains $\dot{\varepsilon}_{ij}^p$:

$$\dot{\varepsilon}_{ij}^p = \dot{\lambda} \frac{\partial G(\sigma_{mn}; \kappa^p)}{\partial \sigma_{ij}} \quad (3)$$

where $\dot{\lambda}$ is the plastic consistency factor, G is the plastic potential function.

The plastic hardening variable κ^p is obtained normalizing energy dissipated by the plastic process to unity and varies from 0, for the virgin material, to 1, when the maximum energy is plastically dissipated. The original definition in Ref. [21] has been modified to take into account the plastic energy dissipation process under triaxial compression.

$$\dot{\kappa}^p = \left[\frac{r}{g_f^{*p}} + \frac{(1-r)}{g_c^{*p}} \right] \sigma_{ij} \dot{\varepsilon}_{ij}^p = \dot{\lambda} h_{ij}^p \frac{\partial G}{\partial \sigma_{ij}};$$

$$h_{ij}^p = \left[\frac{r}{g_f^{*p}} + \frac{(1-r)}{g_c^{*p}} \right] \sigma_{ij} \quad (4)$$

where r represents a measure of the ratio between tensile and compressive stresses and can be evaluated as follows,

$$r = \frac{\sum_{i=1}^3 \langle \sigma_i \rangle}{\sum_{i=1}^3 |\sigma_i|} \quad \langle \sigma_i \rangle = \frac{1}{2} [\sigma_i + |\sigma_i|] \quad (5)$$

σ_i are the principal stresses.

$$g_f^{*p} = \left(\frac{\sum_{i=1}^3 |\sigma_i| R^{op}}{f^p(\sigma_{ij})} \right)^{1+H(-r)} g_f^p$$

$$g_c^{*p} = \left(\frac{\sum_{i=1}^3 |\sigma_i|}{f^p(\sigma_{ij})} \right)^{1+H(-r)} g_c^p \quad H(-r) \begin{cases} = 0 & \text{if } r > 0 \\ = 1 & \text{if } r = 0. \end{cases} \quad (6)$$

R^{op} is the relation between the yielding thresholds in uniaxial compression and that corresponding to uniaxial tension; g_f^p and g_c^p are the maximum energy densities dissipated by the plastic process in uniaxial tension and compression processes respectively. In the case of a thermodynamic process with no damage dissipation, they can be evaluated as follows,

$$g_f^p = \frac{G_f}{l_c} \quad \text{and} \quad g_c^p = \frac{G_c}{l_c} \quad (7)$$

where G_f and G_c are the fracture and crushing energies respectively [22] and l_c is an external parameter that depends on the characteristic size of the finite element mesh. This parameter is introduced in order to obtain objectivity of the solid response respect to the mesh size [25].

The following evolution equation is proposed for the equivalent yielding threshold [21,24]:

$$K(\sigma_{ij}, \kappa^p) = r\sigma_t(\kappa^p) + (1-r)\sigma_c(\kappa^p) \quad (8)$$

where $\sigma_t(\kappa^p)$ and $\sigma_c(\kappa^p)$ represent the evolution of the yielding threshold in uniaxial tension and compression tests

Loading/unloading conditions are derived from the Kuhn–Tucker relations formulated for problems with unilateral restrictions:

$$\dot{\lambda} \geq 0 \quad F^p \leq 0 \quad \dot{\lambda} F^p = 0. \quad (9)$$

3.2. Damage process

The damage threshold is described by a damage function in the following way [21,24]:

$$F^d = f^d(\sigma_{ij}) - K^d(\sigma_{ij}, \kappa^d) = 0 \quad (10)$$

where $f^d(\sigma_{ij})$ is the equivalent tension, $K^d(\sigma_{ij}, \kappa^d)$ is the equivalent damage threshold and κ^d is the degradation variable.

The equivalent tension $f^d(\sigma_{ij})$ can be evaluated using known yielding functions (Tresca, Von-Mises, Mohr–Coulomb or Drucker–Prager) or any function specially developed for damage.

The degradation variable κ^d varies from 0, for the virgin material, to 1, for the completely damaged material and is obtained normalizing energy dissipated by damage to unity [21, 24],

$$\dot{\kappa}^d = \left[\frac{r}{g_f^{*d}} + \frac{(1-r)}{g_c^{*d}} \right] \Psi^o \dot{d} = h^d \dot{d};$$

$$h^d = \left[\frac{r}{g_f^{*d}} + \frac{(1-r)}{g_c^{*d}} \right] \Psi^o \quad (11)$$

$$g_f^{*d} = \left(\frac{\sum_{i=1}^3 |\sigma_i| R^{od}}{f^d} \right)^{1+H(-r)} g_f^d;$$

$$g_c^{*d} = \left(\frac{\sum_{i=1}^3 |\sigma_i|}{f^d} \right)^{1+H(-r)} g_c^d. \quad (12)$$

R^{od} is the relation between the damage thresholds in uniaxial compression and that corresponding to uniaxial tension and g_f^d and g_c^d are the maximum energy densities dissipated by damage in uniaxial tension and compression processes [21,24].

The following evolution equation is proposed for the equivalent damage threshold [21,24],

$$K^d(\sigma_{ij}, \kappa^d) = r\sigma_t(\kappa^d) + (1-r)\sigma_c(\kappa^d) \quad (13)$$

where $\sigma_t(\kappa^d)$ and $\sigma_c(\kappa^d)$ represent the evolution of the damage threshold in uniaxial tension and compression tests respectively.

The loading/unloading conditions are derived from the Khun–Tucker relations and are analogous to the ones corresponding to the plastic process:

$$\dot{d} \leq 0 \quad F^d \leq 0 \quad \dot{d} F^d = 0. \quad (14)$$

3.3. Consistency conditions

Evolution of permanent strains and damage is obtained from the simultaneous solution of the following equations called the *consistency conditions* of the problem:

$$\begin{cases} \dot{F}^p = 0 \\ \dot{F}^d = 0. \end{cases} \quad (15)$$

Eq. (15) are two linear equations in $\dot{\lambda}$ and \dot{d} that can be easily solved.

3.4. Yielding function

The elastic threshold criterion proposed for concrete is a modification of the Lubliner–Oller [22,26] criterion to reproduce the behaviour of concrete under high hydrostatic pressures. In order to have curve meridians [27] a second-degree function of the first invariant was introduced:

$$F^p = \sqrt{3}J_2 + \alpha I_1 + \beta \langle \sigma^{\max} \rangle - \gamma \langle -\sigma^{\max} \rangle$$

$$+ \frac{\delta}{\sigma_c(\kappa^p)} (1-\alpha) I_1^2 - \sigma_c(\kappa^p) (1+\alpha)(1+\delta) \leq 0 \quad (16)$$

where α , β , γ and δ are constants that define the shape of the yielding function, I_1 is the first invariant of the stress tensor, J_2 is the second invariant of the deviatoric stress tensor, σ^{\max} is the maximum principal stress.

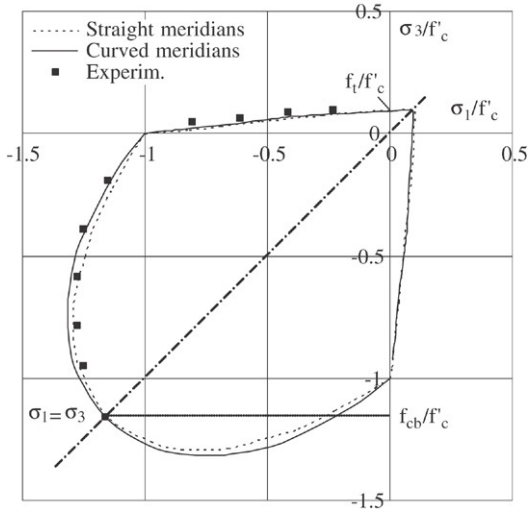


Fig. 1. Proposed yielding surface — Plane $\sigma_2 = 0$. Comparison with experimental results [28].

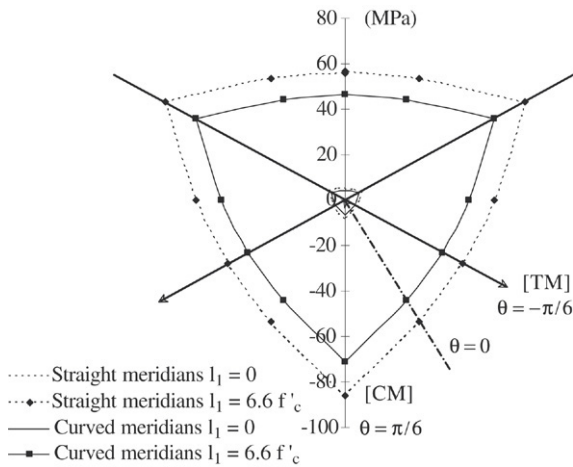


Fig. 2. Proposed yielding surface — Octahedral plane.

Parameter α takes into account the relation between strength in uniaxial compression f'_c and biaxial compression f_{cb} , $R_{cb} = f_{cb}/f'_c$, see Fig. 1. The shape of the yielding surface on plane $\sigma_2 = 0$ and its comparison with the original surface with straight meridians [22,26] and experimental results by Kupfer et al. [28] are presented in Fig. 1.

Parameter β takes into account the ratio between the strength in uniaxial compression f'_c and uniaxial tension f_t , $R^0 = f'_c/f_t$.

Parameter γ is a function of the ratio between maximum octahedral radius in compression and tension r_{oct}^{max} and appears only in triaxial compression states, i.e. $\sigma_3 \leq \sigma_2 \leq \sigma_1 = \sigma^{max} \leq 0$. The ratio between octahedral radius is constant along the hydrostatic axis and between the range $0.5 \leq r_{oct}^{max} \leq 1.0$.

Fig. 2 shows the shape of the proposed elastic threshold in octahedral planes corresponding to different octahedral stresses. It is represented by a convex curve with three corners corresponding to the three compression meridian planes.

Parameter $\delta \geq 0$ is related to the curvature of the meridians. The ultimate surface can be used to define δ , if

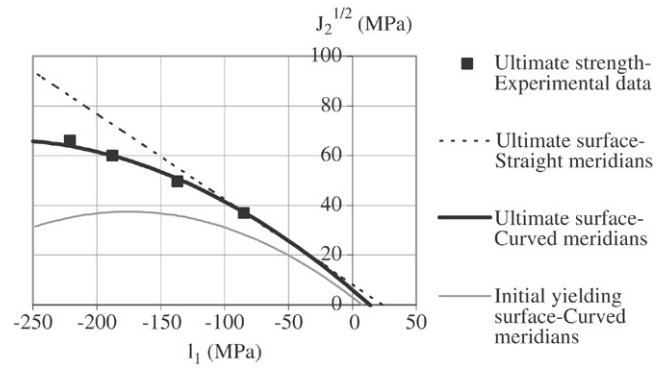


Fig. 3. Proposed yielding and ultimate strength surfaces — Compression meridian plane. Comparison with triaxial compression experimental results [29].

the compression meridian is forced to pass through the point corresponding to a triaxial compression with p_h hydrostatic pressure and σ_{cu} compression strength under that confinement as shown in Fig. 3. For $\delta = 0$ the original yielding criterion of Lubliner–Oller [26] with straight meridians is recovered. Experimental results by Sfer [29] are also plotted on Fig. 3 in order to show that they can be approximately reproduced by the second order polynomial proposed.

The same value of parameter δ obtained for the ultimate strength can be used for the elastic threshold. As a result, the curve describing the initial elastic threshold has more curvature than that defining the ultimate strength. This fact is in accordance with experimental results which show that the difference between the elastic limit and the ultimate strength grows with hydrostatic pressure. See Fig. 3.

The function described by Eq. (16), with curve meridians, can also be used as a plastic potential function to control dilatation for high confinement pressures. A Von Mises function can be used to describe damage due to changes in porous structure of concrete taking place under high confining pressures.

3.5. Model parameters

The model proposed includes many parameters because it has been conceived as a general model that can be calibrated for different types of materials by setting appropriate values for the parameters. Nevertheless, as the paper is focused on the application to concrete, some guides on how to obtain the parameters for concrete are given below [30].

The parameters used for the model depend on the type of concrete and they are valid for any kind of stress combination. Most of the parameters of concrete depend on the compressive strength f'_c and the other parameters take almost fix values. The compression strength is the key value for the model. The model cannot be calibrated without this value.

The elasticity modulus and Poisson's ratio of concrete can be obtained from a uniaxial compression test. Nevertheless, there are many empirical equations that could be used for the estimation of the elasticity modulus as a function of the compressive strength f'_c , in case the stress–strain curve for the

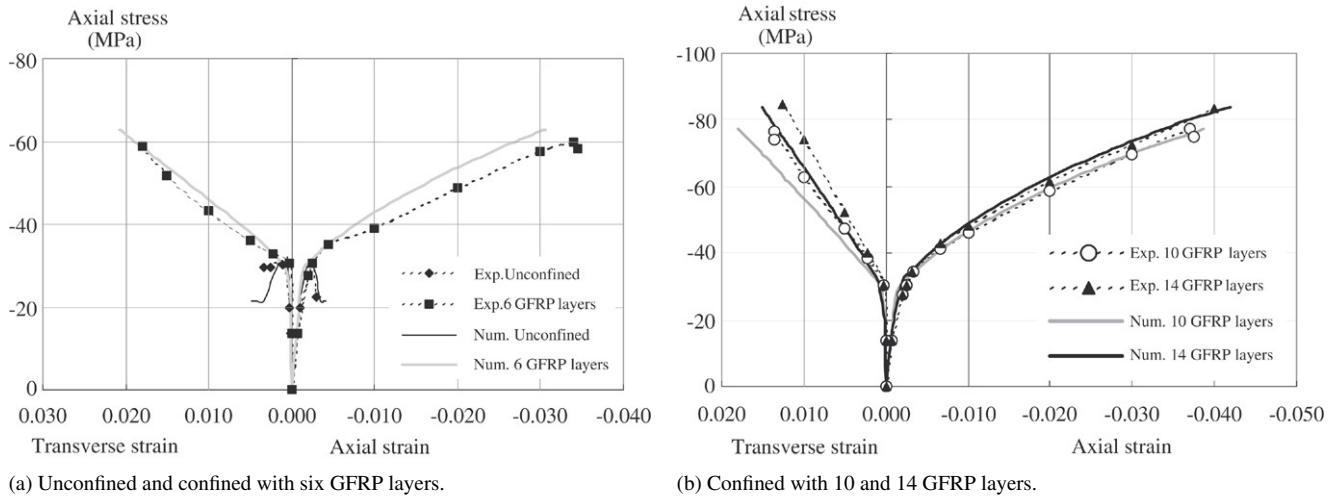


Fig. 4. Stress–strain response of GFRP confined concrete. Comparison with experimental results [16].

uniaxial test is not available. The Poisson's ratio of concrete can be approximate as 0.19 or 0.20 [22].

The compression elastic limit can be obtained from the stress–strain curve of a uniaxial compression test. For the sake of simplicity, the behaviour can be supposed to be elastic up to the discontinuity level that is defined as the point at which the Poisson's ratio begins to increase and occurs at about 75% of the ultimate strength [22].

The plastic damage variable for the peak stress κ_{comp}^p can be obtained from an uniaxial compression stress–strain curve but it always ranges from 0.1 to 0.20.

The compression/tension strength ratio, $R^0 = f'_c/f'_t$ can be obtained if uniaxial compression and tension strengths are available. According to experimental results [28], the value of R^0 is 9.1, 11.1 and 12.5 for compressive strengths of 19 MPa, 32 MPa and 60 MPa respectively and can be approximate as 10 for a normal strength concrete.

The biaxial compression/uniaxial compression strength ratio $R_{cb} = f_{cb}/f'_c$ can be obtained from biaxial tests [28] and it ranges from 1.10 to 1.16.

Experimental results indicate that $r_{\text{oct}}^{\text{max}}$ tends to a constant value of about 0.65, from which results $\gamma = 3.5$ [22,26].

The compression meridian's curvature is defined from triaxial compression tests results. If these results are not available, there are many empirical equations for the prediction of compressive strength as a function of confinement pressure [18].

Fracture energy of concrete can be obtained from three point bend tests on notched beams [31]. It ranges from 100 to 300 Pa m [19]. Crushing energy [19] can be approximated as: $G_c \approx (R^0)^2 G_f$.

The damage threshold in uniaxial compression can be obtained from a cyclic compression test but, according to application examples presented later, it can be approximately taken as $0.90f'_c$. The damage hardening curve $\sigma_c(\kappa^d)$ can be obtained from uniaxial cyclic tests but it can be approximated as linear with a slope equal to 0.008–0.015E.

4. Application examples

4.1. Introduction

The model previously described was implemented in a nonlinear finite element plane code. This program was used for the numerical simulation of the behaviour of concrete and reinforced concrete columns confined with fibre CFRP and GFRP and reinforced concrete beams retrofitted with FRP laminas.

The concrete model parameters are obtained from uniaxial compression data. In all the cases the compression strength is given in the papers from which experimental results were obtained. Some of them include the value of the elastic modulus. When it is not available it is estimated by the empirical equations suggested in Section 3.5. The rest of the mechanical properties were estimated following the guidelines given in Section 3.5.

The composite is modelled as an orthotropic elastic brittle material for compression tests, while an isotropic elastic brittle law is enough to model flexural tests because in this case the composite only works in fibres' direction.

4.2. Behaviour cylindrical concrete filled GFRP tubes under compression

Cylindrical (152.5 × 305 mm) concrete filled GFRP tubes were analyzed [16]. The mechanical properties of concrete are condensed in Table 1. FRP tubes consist of a filament-wound angle ply of polyester resin with unidirectional E-Glass fibres at $\pm 15^\circ$ winding angle. Three distinct jacket thicknesses of 6, 10 and 14 plies (layers) were tested. The thickness, hoop strength and modulus of elasticity of the FRP tubes are presented in Table 2.

Stress–strain curves and volumetric response obtained for plain concrete and the three types of FRP tubes are plotted in Figs. 4 and 5, together with experimental results corresponding to batch C [16]. The predicted response matches experimental results in all cases. Fig. 6 shows the dilatation response curves

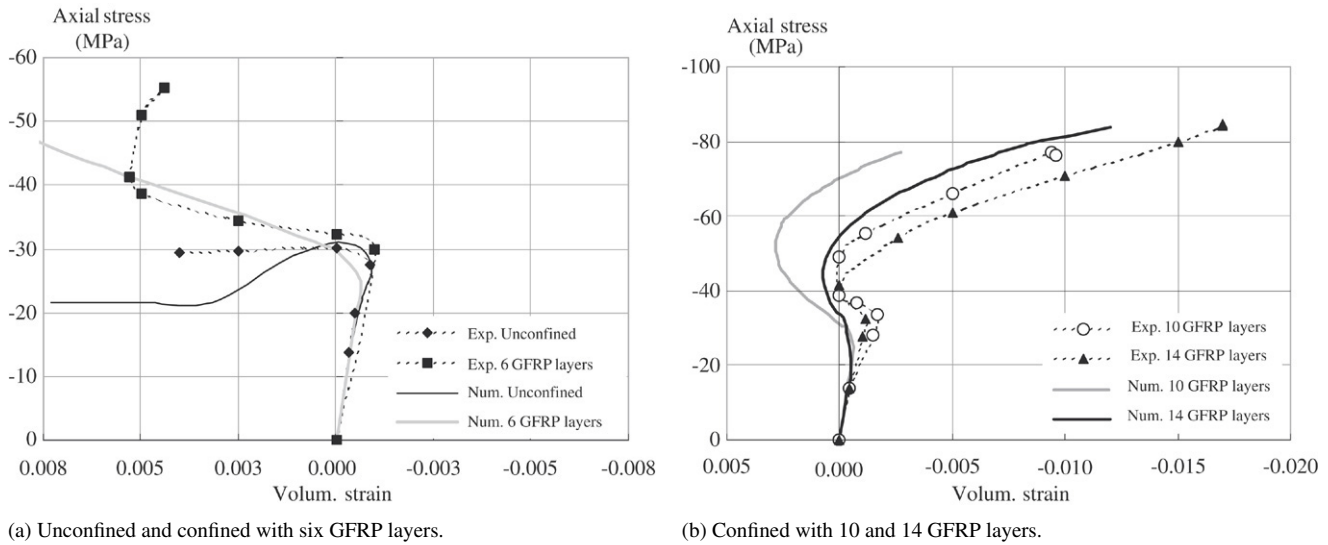


Fig. 5. Volumetric response of GFRP confined concrete. Comparison with experimental results [16].

Table 1
Mechanical properties of concrete [16,32,33,10,34,5]

Properties	Test by Mirmiran and Shahawy [16]	Test by Lin and Liao [32]	Test by Demers and Neale [33]		Tests by Buyle-Bodin et al. and David et al. [10,34]	Test by Ahmed et al. [5]
			C1	C2		
Elasticity modulus, E	23 273 MPa	23 148 MPa	25 800 MPa	22 300 MPa	29 000 MPa	30 000 MPa
Poisson ratio, ν	0.2	0.2	0.2	0.2	0.2	0.2
Compression ultimate strength, σ_{uc}	31 MPa	23.91 MPa	25 MPa	25 MPa	40 MPa	41 MPa
Uniaxial compression elastic threshold, σ_{fc}	28 MPa	18 MPa	15 MPa	15 MPa	20 MPa	27 MPa
Elastic threshold ratio, R_0^p	8	8	8	8	10	10
R_{bc}	1.16	1.16	1.16	1.16	1.16	1.16
γ	3	3	3	3	3	3
Confined compression						
p_h	30 MPa	30 MPa	30 MPa	30 MPa	30 MPa	30 MPa
σ_{ccu}	120 MPa	91 MPa	91 MPa	91 MPa	91 MPa	91 MPa
Plastic damage variable for the peak stress, κ_{comp}^p	0.15	0.15	0.15	0.15	0.20	0.20
Crushing energy, G_c^p	1.5E-2 MPa m	1.0E-2 MPa m	1.E-2 MPa m	1.2E-2 MPa m	2.5E-2 MPa m	3.2E-2 MPa m
Fracture energy, G_f^p	1.5E-4 MPa m	1.0E-4 MPa m	1.E-4 MPa m	1.2E-4 MPa m	2.5E-4 MPa m	3.2E-4 MPa m
Uniaxial compression damage threshold, σ_c^d	30 MPa	23 MPa	20 MPa	20 MPa	39 MPa	40 MPa
Damage hardening slope	190 MPa	270 MPa	300 MPa	270 MPa	320 MPa	330 MPa

for plain concrete and for the different thickness of FRP confinement. Numerical results show the same variation of experimental ones in all cases. Dilatational effect is reversed by the confinement and the dilatation rate reaches a maximum, then decreases and finally stabilizes at an asymptotic value.

To evaluate stiffness degradation and compare it with experimental results, a cyclic compression test of 14-layer

specimen (DA32) was reproduced. The specimen was subjected to four unloading–reloading cycles. The stress–strain response obtained with the proposed model and that recorded in the test are plotted in Fig. 7. It can be concluded that, although the numerical model is not able to reproduce the loops registered in the tests, it accurately reproduces the average stiffness degradation due to damage.

Table 2
Mechanical properties of FRPs [16,32,33,10,34,5]

Properties	Tests by Mirmiran and Shahawy [16] GFRP	Tests by Lin and Liao [32] GFRP		Tests by Demers and Neale [33] CFRP	Tests by Buyle-Bodin et al. and David et al. [10,34] CFRP	Buyle-Bodin et al. [10] GFRP	Test by Ahmed et al. [5] CFRP
		1 layer	2 layers				
Longitudinal elasticity modulus, E_l	37 233 MPa	238 253 MPa	224 579 MPa	84 000 MPa	150 000 MPa	11 700 MPa	240 000 MPa
Transversal elasticity modulus, E_t	12 400 MPa	7942 MPa	7486 MPa	10 500 MPa	–	–	–
Longitudinal–transversal Poisson ratio, ν_{lt}	0.26	0.26	0.26	0.23	0.29	0.28	0.33
Transversal–longitudinal Poisson ratio, ν_{tl}	0.1	0.1	0.1	0.032	0.29	0.28	0.33
Transversal–transversal Poisson ratio, ν_{tt}	0.29	0.29	0.29	0.30	0.29	0.28	0.33
Circumferential tensile strength, σ_{long}^u	524 MPa	455.44 MPa	403.14 MPa	873 MPa	–	–	–
Tensile strength, σ_t	–	–	–	–	2400 MPa	55 MPa	3500 MPa
Layer thickness	0.21 mm	1.84 mm	3.89 mm	0.3 mm	1.2 mm	6 mm	0.167 mm

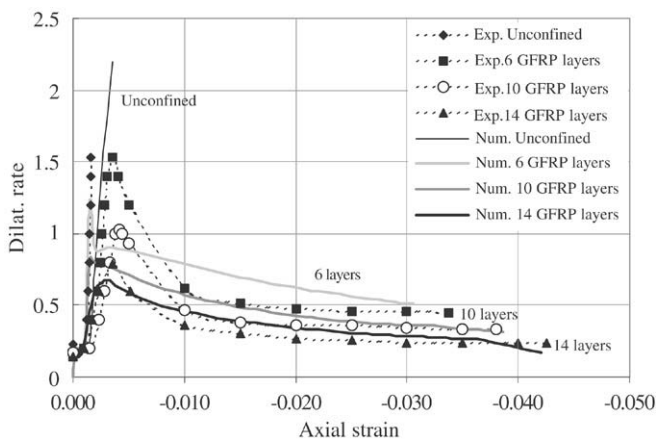


Fig. 6. Dilatation ratio curves for GFRP-confined concrete. Comparison with experimental results [16].

4.3. Compressive strength of reinforced concrete columns confined by glass composites

The proposed model is used here for the evaluation of the strength of six sets of tests carried out over concrete and reinforced concrete columns confined by glass composites [32]. The dimensions of the concrete columns are 100 mm × 200 mm and the diameter of the reinforcing steel bars is 3.5 mm. Concrete was modelled as an elastic–plastic damaged material with mechanical properties presented in Table 1. Only one quarter of the cylindrical specimen was modelled with axial symmetrical finite elements. Glass composite was modelled as an elastic brittle orthotropic material with the mechanical properties presented in Table 2. Steel was modelled as an elastic–plastic hardening material with the mechanical properties presented in Table 3. Bar buckling was

not considered. Table 4 shows the reinforcement of every set of experiments and summarizes the experimental [32] and numerical results in terms of fracture stresses. Comparison between experimental stress and the stress predicted using the model proposed indicates that the present model can predict the fracture stress of FRP-wrapped concrete columns with good accuracy.




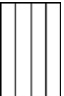
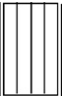

4.4. Behaviour of CFRP confined reinforced concrete columns

Circular reinforced concrete columns confined with carbon fibre reinforced polymers, subjected to monotonic axial loading, were studied [33] using the proposed model. The dimensions of the columns and the reinforcement are indicated in Fig. 8. Due to symmetry only one quarter of each column was modelled. Fig. 8 shows the finite element mesh used. Concrete was modelled as an elastic–plastic damaged material with mechanical properties indicated in Table 1. A bilinear curve with strain hardening was used to model steel in compression and tension. Mechanical properties of steel are summarized in Table 3. Bar buckling was not considered. CFRP was modelled as an elastic brittle orthotropic material with mechanical properties presented in Table 2. The axial stress–axial strain curves for the two columns modelled are presented and compared with experimental results in Fig. 9. The numerical curves can match the experimental ones with reasonable accuracy [33], showing thus the capability of the proposed model to reasonably predict pre and post-peak behaviour, stiffness degradation and strength enhancement. It can also be seen that the predicted peak strain is coincident with the experimental peak strain in both cases.

Table 3
Mechanical properties of steel [32,33,10,34,5]

Properties	Test by Lin and Liao [32]	Test by Demers and Neale [33]	Tests by Buyle-Bodin et al. and David et al. [10,34]	Test by Ahmed et al. [5]	
				$\phi 6$	$\phi 8$
Elasticity modulus, E	212 405 MPa	200 000 MPa	200 000 MPa	195 000 MPa	185 000 MPa
Poisson ratio, ν	0.3	0.3	0.3	0.3	0.3
Yielding stress, σ_f	422.97 MPa	400 MPa	500 MPa	553 MPa	568 MPa
Yielding function	Von Mises	Von Mises	Von Mises	Von Mises	Von Mises
Plastic potential function	Von Mises	Von Mises	Von Mises	Von Mises	Von Mises

Table 4
Comparison of numerical strength with experimental results [32]

Name	C1 ^a	C2 ^b	C3 ^c	C4 ^d	C5 ^e	C6 ^f
Figure						
Experimental stress (MPa)	23.91	61.98	91.08	31.92	70.00	102.36
Numerical stress (MPa)	23.97	62.06	89.27	31.25	69.32	101.97
Num./Exp.	1.002	1.001	0.980	0.979	0.990	0.996

^a Plain Concrete.

^b Plain Concrete confined by 1GFRP layer.

^c Plain Concrete confined by 2 GFRP layers.

^d Axial RC.

^e Axial RC confined by 1 GFRP layer.

^f Axial RC confined by 2 GFRP layers.

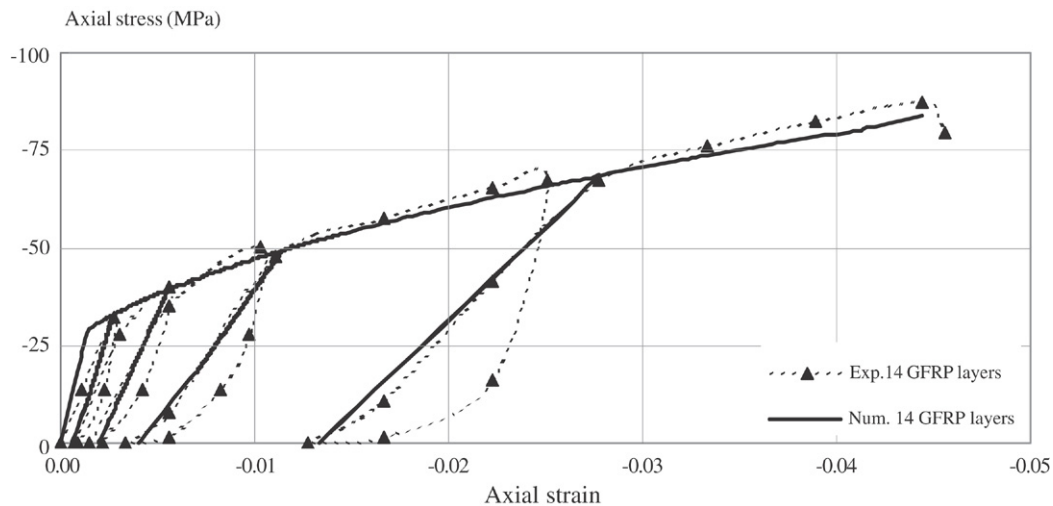


Fig. 7. Uniaxial cyclic response of GFRP-encased concrete under compression. Comparison with experimental results [16].

4.5. Flexural behaviour of externally bonded FRPs reinforced concrete beams

Simple supported RC beams with and without external FRP reinforcement and loaded monotonically in four points bending moment are considered here [10,34]. Four specimens were analyzed: an unstrengthened RC beam, called control beam, two RC beams externally bonded with one and two layers of CFRP sheets and a RC beam strengthened with a GFRP plate. CFRP sheets consisted of unidirectional carbon fibres, while GFRP plate was a glass fibre mat (short fibres

arranged in all directions). The geometry of the beams and arrangement of the different FRP reinforcements are shown in Fig. 10. A two-dimensional plane-stress analysis was carried out. Concrete was modelled as an elastic–plastic damaged material with the mechanical properties presented in Table 1. A perfectly elastic–plastic law with hardening was used for the steel bars, and an isotropic elastic brittle law was sufficient to model FRP reinforcement because it is only working in fibres direction. Mechanical properties of steel and FRPs are indicated in Tables 2 and 3. Fig. 11(a) and (b) show experimental [10, 34] and numerical load-vs-deflection curves for RC beams

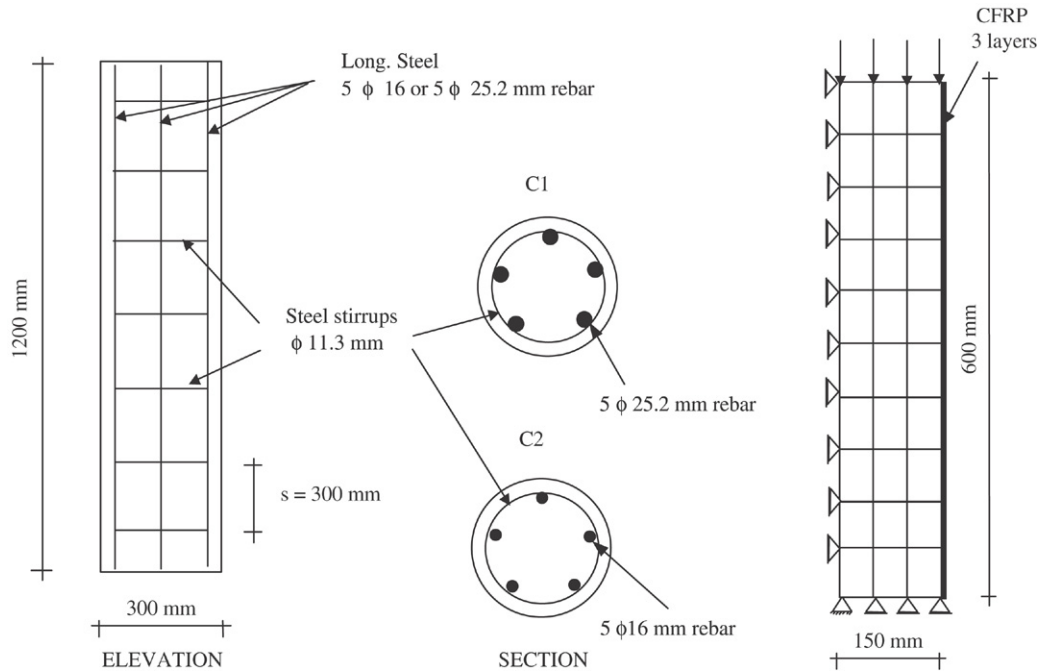


Fig. 8. Details of reinforced concrete columns [32] and finite element used for the analysis.

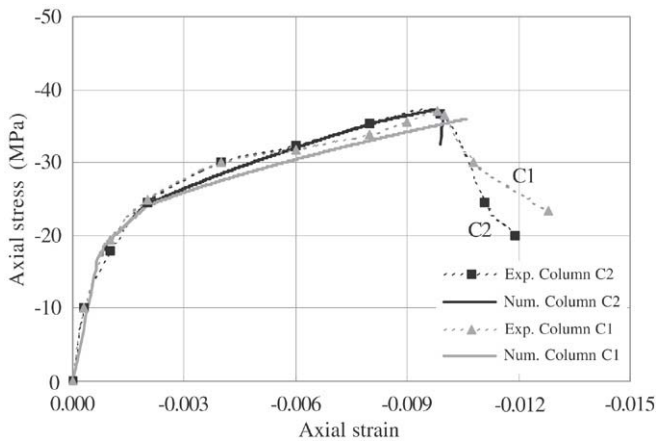


Fig. 9. Axial stress–axial strain curve for CFRP RC columns. Comparison with experimental results [32].

strengthened with CFRP sheets and GFRP plate respectively. The finite element mesh used in all cases can also be seen in Fig. 11(a). Numerical curves predict with good agreement not only the response of control beam but also the behaviour of FRP strengthened beams. In this sense the model was able to reproduce the significant increase in flexural stiffness and ultimate capacity achieved by those beams. FRP strengthened beams failed in a brittle manner, while control beam failed due to concrete crushing. These failure modes of concrete, called shear and crushing failure, were reasonable reproduced by the present model, as can be seen in Fig. 11(a) and (b).

4.6. Flexural behaviour of externally bonded CFRP reinforced concrete beams with different unsheeted lengths

Simple supported RC beams tested under two point loading bending are studied [5]. Three beams were analyzed: an

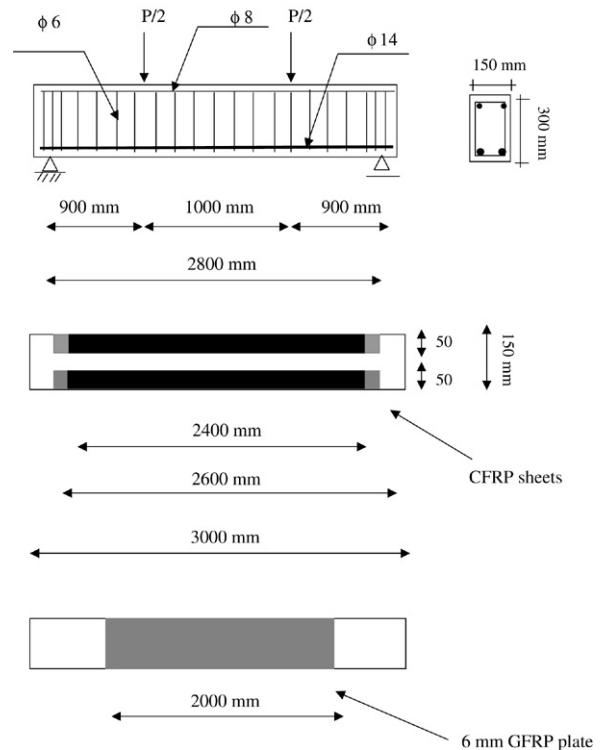


Fig. 10. Details of RC beams and arrangement of different FRP reinforcements [10,33].

unstrengthened RC beam, called control beam, and two RC beams strengthened with two layers of longitudinal CFRP laminates bonded symmetrically onto the bottom of their surface. The parameter taken into account here is the distance between the cut-off point of the CFRP laminates and the nearer support, the so-called unsheeted length [5]. Hence two unsheeted lengths were considered: $L = 150$ mm, $L = 100$ mm.

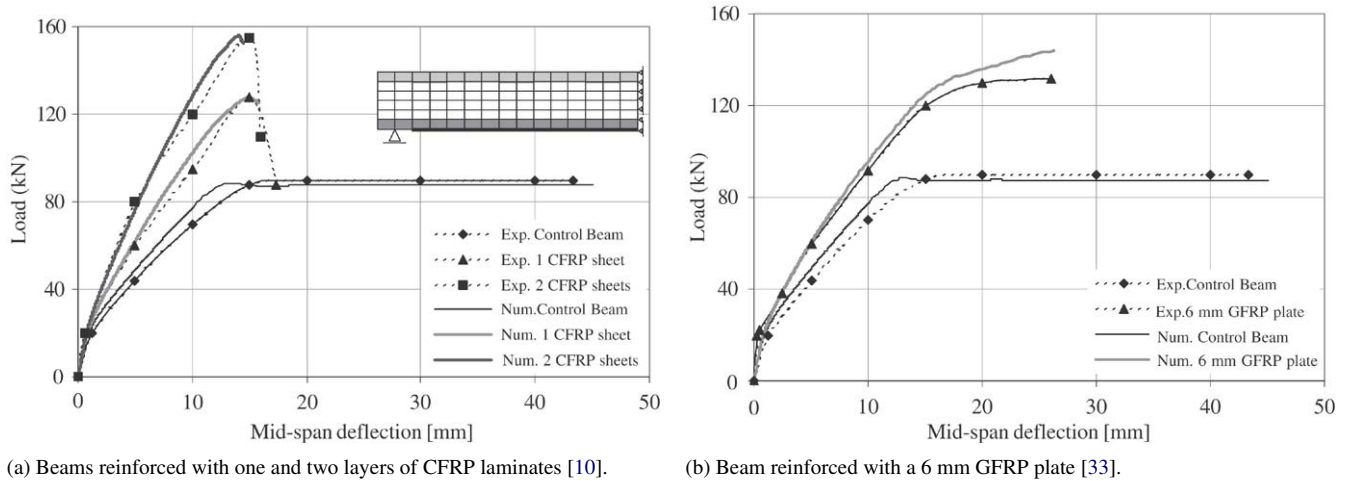


Fig. 11. Load-vs-mid-span deflection for RC beams reinforced with different FRP composites sheets. Comparison with experimental results [10,33].

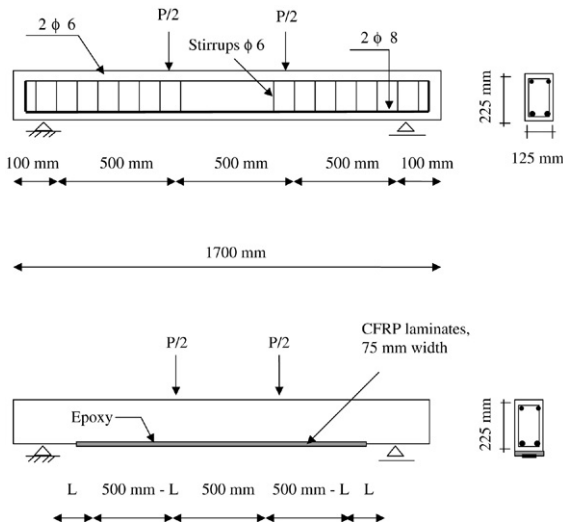


Fig. 12. Details of RC beams and arrangement of CFRP reinforcement [5].

Geometry of the control beam and the reinforced beams and the arrangement of CFRP laminates are shown in Fig. 12. Concrete, steel and CFRP laminates were modelled using the same laws as in example 4.5 and mechanical properties of these materials are summarized in Tables 1–3 respectively. A two-dimensional plane-stress analysis was performed. The finite element mesh used can be observed in Fig. 13. Experimental [5] and numerical total load applied vs mid-span deflection curves for control beam and CFRP strengthened beams are shown in Fig. 13. Numerical curves can reproduce with good accuracy the ultimate rupture load and the increase in stiffness and strength achieved by strengthened beams, as well as the behaviour of control beam. In addition, the failure modes of all specimens, the flexural one for control beam and shear failure for strengthened beams, could be predicted by the model with reasonable accuracy.

5. Conclusions

A numerical simulation of reinforced and unreinforced concrete columns and RC beams retrofitted with FRP laminates

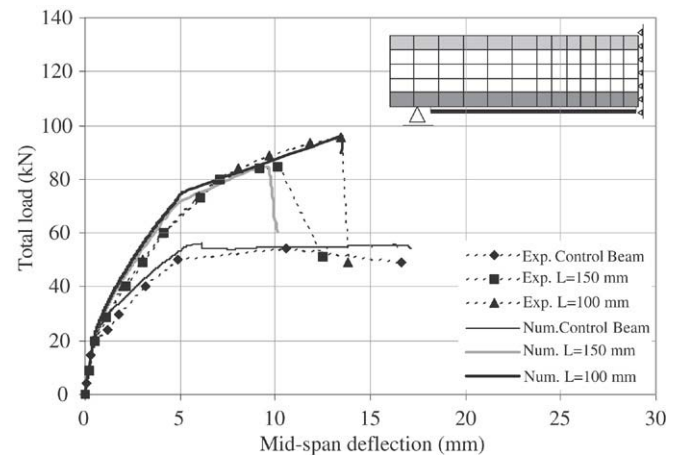


Fig. 13. Load-vs-mid-span deflection for RC beams of different unsheeted lengths *L*.

was carried out using the plastic damage model presented. The following conclusions can be derived from the analysis:

The model presented accurately reproduces the behaviour of confined concrete, not only in the axial direction but also in the transverse one, as well as the response of flexural concrete members.

The adequate computation of transverse strains in confined concrete columns plays a crucial role in the evaluation of the FRP retrofitting system. FRP behaves elastically, so the confinement pressure is always increasing until the tensile failure of the FRP layers. As the stress state in the composite mainly depends on the transverse deformation of the concrete core, it might be properly evaluated in order to predict the ultimate load capacity of the retrofitted column.

The numerical response obtained with the plastic damage model is closer to experimental results than that obtained with a plastic model with the same yielding function and hardening variable. The difference between the two types of models is stronger in the case or triaxial compression.

The modification of the plastic hardening variable proposed leads to a better representation of concrete ductility under triaxial compression and shear.

The use of a yielding criteria based on a second-degree function defines a yielding surface with curve meridians that accurately reproduces the variation of compression strength with the confinement pressure. The comparison with experimental results shows that this yielding surface is able to reproduce ultimate strength under compression for a fairly wide range of pressures.

Finally the model was also capable of reproducing the shear and crushing failure of concrete.

Acknowledgements

The financial support of CONICET, CIUNT (National University of Tucumán) and Technological University is gratefully acknowledged. The authors also wish to thank the collaboration of Mrs Amelia Campos in the English revision.

References

- [1] Lopez M. Development of a finite element model of RC beams strengthened with CFRP laminates. Department of Civil and Env. Engineering, Penn State University.
- [2] Khalifa A, Nanni A. Improving shear capacity of existing RC T-section beams using CFRP composites. *Cement & Concrete Composites* 2000; 22:165–74.
- [3] Toutanji H, Deng Y. Strength and durability performance of concrete axially loaded members confined with AFRP composites sheets. *Composites Part B: Engineering* 2002;33:255–61.
- [4] Karabinis AI, Kioussis PD. Plasticity computations for the design of the ductility of circular concrete columns. *Computers & Structures* 1996; 60(5):825–35.
- [5] Ahmed O, Van Gemert D, Vandewalle L. Improved model for plate-end shear of CFRP strengthened RC beams. *Cement & Concrete Composites* 2001;23:3–19.
- [6] Almakt M, Balázs G, Pilakoutas K. Strengthening of RC elements by CFRP plates. Local Failure, 2do. In: *Int. Ph.D. symposium in civil engineering*. 1998.
- [7] Tumialan G, Serra P, Nanni A, Belarbi A. Concrete cover delamination in RC beams strengthened with FRP sheets. *ACI*. In: *Pro., 4th international symposium on FRP for reinforcement of concrete structures*. 1999. p. 725–35.
- [8] Yang Z, Chen J, Proverbs D. Finite element modelling of concrete cover separation failure in FRP plated RC beams. *Construction and Building Materials* 2003;17:3–13.
- [9] Perera R, Recuero A, De Diego A, López C. Adherence analysis of fiber-reinforced polymer strengthened RC beams. *Computers & Structures* 2004;82:1865–73.
- [10] Buyle-Bodin F, David E, Ragneau E. Finite element modeling of flexural behavior of externally bonded CFRP reinforced concrete structures. *Engineering Structures* 2002;24:1423–9.
- [11] Ramana V, Kant T, Morton S, Dutta P, Mukherjee, Desai Y. Behavior of CFRPC strengthened reinforced concrete beams with varying degrees of degrees of strengthening. *Composites Part B: Engineering* 2000;31: 461–70.
- [12] Wang Y, Chen C. Analytical study on reinforced concrete beams strengthened for flexure and shear with composite plates. *Composite Structures* 2003;59:137–48.
- [13] An W, Saadatmanesh H, Eshani M. RC beams strengthened with FRP plates, II: Analysis and parametric study. *Journal of Structural Engineering ASCE* 1991;117(11):3434–54.
- [14] Van Den Einde L, Zhao L, Seible F. Use of FRP composites in civil structural applications. *Construction and Building Materials* 2003;17: 389–403.
- [15] Shahawy M, Mirmiran A, Beitelman M. Tests and modeling of carbon-wrapped concrete columns. *Composites: Part B* 2000;31:471–80.
- [16] Mirmiran A, Shahawy M. Behavior of concrete columns confined by fiber composites. *Journal of Structural Engineering ASCE* 1997;123(5): 583–90.
- [17] Samaan M, Mirmiran A, Shahawy M. Model of concrete confined by fiber composites. *Journal of Structural Engineering ASCE* 1998;124(9): 1025–31.
- [18] Untiveros C. Estudio experimental del comportamiento del hormigón confinado sometido a compresión. Ph.D. thesis. Spain: Universitat Politecnica de Catalunya, Escola Técnica Superior D'Ingenyers de Camins, Canals I Ports; 2002.
- [19] Shahawy M, Beitelman T. Static and fatigue performance of RC beams strengthened with CFRP laminates. *Journal of Structural Engineering* 1999;125:613–21.
- [20] ACI 440.2R-02. Guide for the design and construction of externally bonded FRP systems for strengthening concrete structures. American Concrete Institute. 2002.
- [21] Luccioni BM, Oller S, Danesi R. Coupled plastic damage model. *Computer Methods in Applied Mechanics and Engineering* 1996;129: 81–9.
- [22] Oller S. Un modelo de Daño Continuo para materiales Friccionales. Ph.D. thesis. Spain: Universitat Politecnica de Catalunya, Escola Técnica Superior D'Ingenyers de Camins, Canals I Ports; 2002.
- [23] Lubliner J, Oliver J, Oller S, Oñate E. A plastic damage model for concrete. *International Journal of Solids Structures* 1989;25(3):299–326.
- [24] Luccioni B. Formulación de un modelo constitutivo para materiales ortótropos. Ph.D. thesis. Argentina: Universidad Nacional de Tucumán; 1993.
- [25] Oliver J. A consistent characteristic length for smeared cracking models. *International Journal of Numerical Methods Engineering* 1989; 28:461–74.
- [26] Oller S, Oliver J, Lubliner J, Oñate E. Un modelo constitutivo de daño plástico para materiales friccionales. parte I: Variables fundamentales, funciones de fluencia y potencial. *Revista Internacional de Métodos Numéricos para el Cálculo y Diseño en Ingeniería* 1988;4:397–428.
- [27] Chen W. *Plasticity in reinforced concrete*. Mc Graw Hill; 1982.
- [28] Kupfer H, Hilsdorf H, Rusch H. Behavior of concrete under biaxial stresses. *ACI Journal* 1969;66(8):656–66.
- [29] Sfer D, Carol I, Gettu R, Etsch G. Study of the behavior of concrete under triaxial compression. *Journal of Engineering Mechanics ASCE* 2000; 128(2):156–63.
- [30] Luccioni B, Rougier V. A plastic damage approach for confined concrete. *Computers & Structures* 2005;83:2238–56.
- [31] RILEM. Determination of the fracture energy of mortar and concrete by means of three-point bend test on notched beams. *Materials and Structures* 1985;18(106):285–90.
- [32] Lin H, Liao Ch. Compressive strength of reinforced concrete column confined by composite material. *Composite Structures* 2004;65:239–50.
- [33] Montoya E, Vecchio F, Sheikh S. Numerical evaluation of the behaviour of steel and FRP — confined concrete columns using compression field modelling. *Engineering Structures* 2004;26(11):1535–45.
- [34] David E, Djelal C, Buyle-Bodin F. Repair and strengthening of reinforced concrete beams using composites materials, 2do. In: *Int. Ph.D. symposium in civil engineering*. 1998.